

Octahedral tilting, domain structure and piezoelectricity in perovskites and related ceramics

Ian M. Reaney

Received: 30 May 2006 / Accepted: 8 September 2006 / Published online: 28 February 2007
© Springer Science + Business Media, LLC 2007

Abstract Perovskites and related compounds constitute the majority of commercial piezoelectric ceramics. Typically, most publications note the crystal structure, grain size and properties of piezoelectrics but often very little is reported about their domain and domain wall structure. In many systems, it is the motion or vibration of the domain walls which dominate the piezoelectric and electromechanical coupling coefficients, the so-called extrinsic contribution. This article discusses mechanisms relating to structure and domain wall structure which either suppress or enhance extrinsic contributions. Consideration is given to the ferroic nature of some systems in which octahedral tilt in addition to ferroelectric phase transitions occur. The domain structure at and adjacent to the morphotropic phase boundary in several well-known systems is also discussed.

Keywords Octahedral tilting · Domain structure · Piezoelectricity · Perovskites · Electron microscopy

1 Introduction

It is well known that the piezoelectric properties of ferroelectric ceramics are dominated by contributions from movements of non-180° domain walls [1]. At very low fields, displacement of the domain walls is assumed either to be negligible or to be reversible. In either case, the piezoelectric properties are independent of the external driving field. At higher fields, the displacement of the walls becomes

partially irreversible, resulting in the dependence of the piezoelectric coefficient on the field and in a hysteretic piezoelectric response [2, 3]. Most studies have been concerned with domain wall contributions to the properties of lead zirconate titanate (PZT) and barium titanate ceramics (BaTiO₃) [4]. Donor doped PZT has a Curie point, $T_C \sim 360^\circ\text{C}$ for its morphotropic phase boundary (MPB) composition ($x=0.52$) which limits the operating temperature to $\sim 180^\circ\text{C}$. There are a number of piezoelectric devices in automotive and aerospace applications which require actuation and sensing at higher temperatures than currently available. Eitel et al. [5] predicted that Bi(Me)O₃-PbTiO₃ systems (Me: Sc, In, Y, Yb, etc) would have higher Curie temperatures and enhanced piezoelectric properties in relation to PZT. BiScO₃-PbTiO₃ (BS-PT) exhibits an MPB at 64% PbTiO₃ between an untilted rhombohedral (R3m) and a tetragonal (P4 mm) phase [6]. It has a T_C of $\sim 450^\circ\text{C}$ at the MPB which is considerably higher than that of PZT¹ coupled with a piezoelectric coefficient, $d_{33}=450$ pC/N, comparable to that of PZT [5, 7].

For applications which require yet higher operating temperatures, Aurivillius phases are the materials of choice [8]. Here, the piezoelectric coefficients are low ($d_{33} \sim 20$ pC/N) relative to those of PZT and BS-PT since no MPB is known to exist but the T_c is typically $>550^\circ\text{C}$ [8]. The most common application for such materials are sensors since the d_{33} values are too low for actuation and compounds are typically based on ABi₄Ti₄O₁₅ (A=Sr) [8].

Studies of the domain structures in the context of piezoelectricity of the above compounds are rare but may be performed using diffraction contrast transmission electron microscopy (TEM). In order to discuss sensibly the domain structures of the various compounds described above, an appreciation of the rules relating crystal structures and the crystallographic habit plane of the domains must first be

I. M. Reaney (✉)
Department of Engineering Materials, University of Sheffield,
Sir Robert Hadfield Building, Mappin St,
Sheffield S1 3JD, UK
e-mail: I.M.Reaney@sheffield.ac.uk

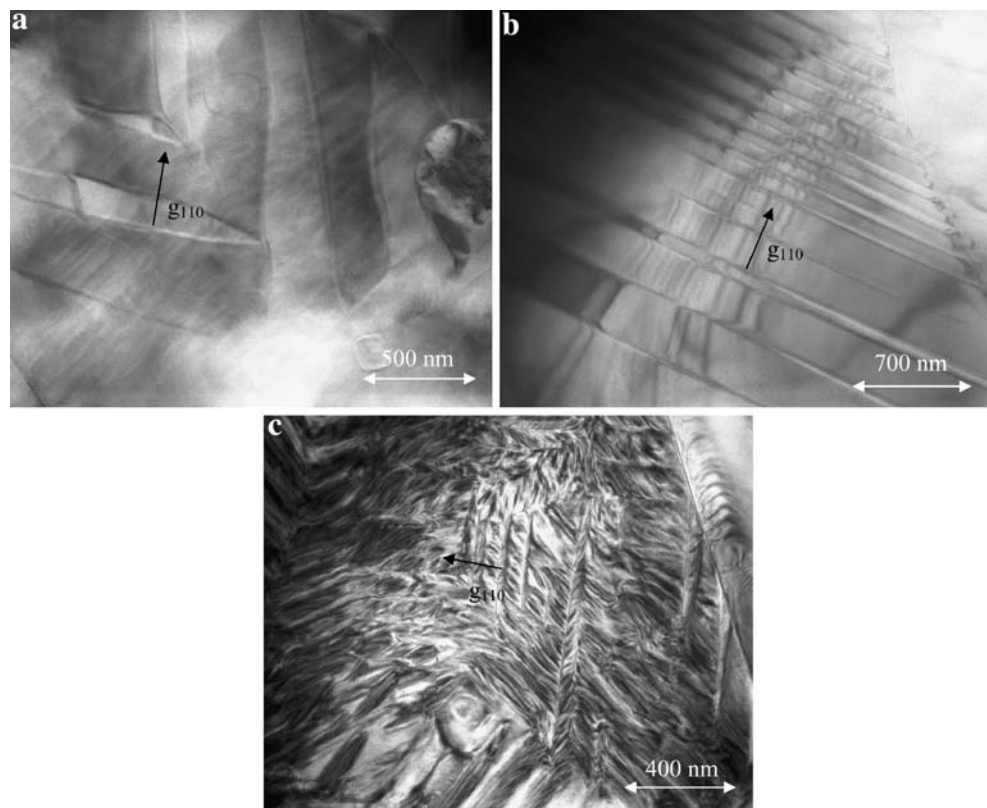
established. For the case of perovskites, the classic ferroelectric phases have tetragonal symmetry (T, $P4mm$) or rhombohedral (R, $R3m$ or $R3c$). For these structures, the non- 180° or orientational domain boundaries (ODB's) which arise due to constraint of the distorting crystal are constricted to lie on either the $\{110\}$ or $\{110\}/\{100\}$ planes for the T and R phase, respectively [9]. For intermediate monoclinic structures such as proposed by Noheda [10] for the MPB in the PZT system, the habit of the domain walls are less well defined and will be related to the specific polarization vector which will control the β angle of the monoclinic structure [9]. There are no restrictions for inversion/ 180° domains nor for translational/antiphase boundaries (APB's). However, APB's formed due to impingement of regions of antiphase octahedral tilting that have nucleated out of phase are often observed to lie normal to the axis of rotation. A plane in which the energy of the APB is intuitively lower since it may be considered as a slab of in-phase tilted material, two unit cells wide, separating antiphase tilted regions.

2 Undoped PZT

Most authors consider the monoclinic phase at the PZT MPB to arise as a result of frustration of the polarization vectors associated with the R and T phases with the mono-

clinic polarization vector lying in the (1–10) plane between the [001] and [111] directions [10, 11]. However, the precise direction is ambiguous and will vary from point to point within the sample in a manner relating to the distribution of the Zr:Ti ratio. Prediction of all the possible domain wall habit planes is therefore problematic. It is more sensible to consider the MPB in the PZT system to be a region in which the domain wall may adopt a habit plane consistent with the local chemistry and therefore structure. In a sample in which the Zr:Ti ratio is well controlled and reasonably homogeneous, Zr and Ti rich clusters will only exist on the order of a few nanometers in diameter. Consequently, the polarization vector may vary over the same scale length. As a result, the distribution of domain walls and their habit planes is anticipated to be complex. Figure 1a, b and c, from a recent publication by Woodward et al. [12] illustrate this point. Samples whose Zr:Ti ratios are far removed from the MPB (R and T phase with $-Zr:Ti$ 60:40 and 40:60, respectively), exhibit a well-organised domain structure stable under irradiation in the electron beam [12]. At the MPB (Zr:Ti ratio 52:48), the domain structure is more ambiguous with a domain size restricted to ~ 20 nm and no simple habit plane for the domain walls. Moreover, despite T_c being in excess of $300^\circ C$, the domain walls are so sensitive to irradiation by the electron beam that determination of the habit planes becomes redundant since they become modified during exposure [12]. The ease with which the

Fig. 1 a, b and c. Domain structures associated with rhombohedral PZT (60/40) tetragonal PZT (40/60) and MPB PZT (52/48), after Woodward et al. [12]



domain walls may be rearranged is consistent with a large extrinsic piezoelectric response in the vicinity of the MPB.

Several workers have attempted to use convergent beam diffraction to directly ascertain if monoclinic symmetry persists at the MPB [13]. To date, such experiments have failed to find monoclinic symmetry and invariably indicate the presence of tetragonal phase [13]. However, such experiments are self-selecting. Convergent beam nano-diffraction requires a stable region of single crystal ceramic in order to ascertain local point group symmetry. The largest most stable domains (>50 nm) in any MPB sample are therefore most attractive from an experimental perspective but these are least likely to be monoclinic and most likely to be tetragonal whose domain structure is stabilized by strong ferroelastic/electric coupling [14]. Therefore, in selecting large coherently diffracting regions, the researchers have biased their data in favour of tetragonal symmetry. However, with the use of ever smaller probe sizes and more intense electron beams, this approach may well yield categorical proof of the presence of monoclinic phase in a single domain at the MPB.

In addition to discussing domain structure, Woodward et al. [12] reviewed the structure of the MPB at low temperature and in agreement with several other authors demonstrated that the monoclinic C_m phase determined by Noheda [10] transforms below $\sim 150^\circ\text{C}$ to a structure in which the oxygen octahedra rotate in antiphase around the polarization vector, resulting in C_c symmetry. The electron diffraction patterns obtained by Woodward et al. [12] are reproduced here but are similar to those attributed to Ragini et al. [15] and Ranjan et al. [16], Fig. 2a and b. The onset of a tilt transition at low temperatures is irrelevant to the piezoelectric properties of undoped PZT which are conventionally recorded at room temperature or above to imitate device conditions. However, PZT is often doped in order to enhance the piezoelectric coefficient by decreasing T_c . These so-called soft PZT's often but not exclusively contain SrO

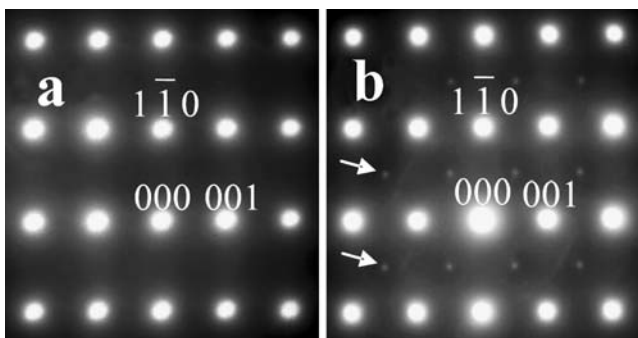


Fig. 2 a and b. $\langle 110 \rangle$ zone axis electron diffraction patterns from MPB PZT at RT and 16 K, respectively, after Ragini et al. [15] and Ranjan et al. [16]. Superlattice reflections of the type $1/2\{000\}$ associated with antiphase tilting are arrowed

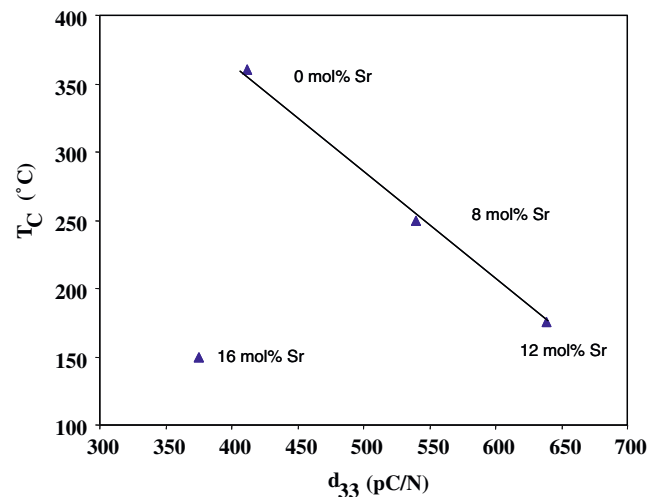


Fig. 3 d_{33} vs T_c for a sequence of MPB Sr doped compositions, after Zheng et al. [17]

substituted for PbO in addition to a small concentration of donor dopants on the A or B-sites. The following section reviews the structure of Sr doped soft PZT and its relation to piezoelectric properties.

3 Sr doped soft PZT

Figure 3 shows d_{33} vs T_c for a sequence of MPB Sr doped compositions initially published by Zheng et al. [17] The value of d_{33} increases with increasing Sr^{2+} concentration until a maximum of ~ 640 pC/N is reached for $x=0.12$. This is followed by a decrease in d_{33} to only ~ 375 pC/N for $x=0.16$. The increase in d_{33} is commensurate with the decrease in T_c until $x=0.12$ but the decrease in d_{33} for $x=0.16$ does not fit this trend [17, 18]. The value of d_{33} for $x=0.16$ therefore disagrees with the accepted premise that a lower T_c should reduce the activation energy for domain wall motion at room temperature, thereby softening the material [17, 18].

Figure 4 shows electron diffraction patterns along pseudocubic $\langle 110 \rangle$ zone axes of MPB samples as a function of Sr^{2+} concentration ($x=0, 0.08, 0.12, 0.16$). For simplicity and direct comparison an indexation based on the pseudocubic simple perovskite unit cell is used. The most intense reflections in these four patterns can be indexed according to the fundamental perovskite structure with $a \sim 0.40$ nm, consistent with the presence of tetragonal/rhombohedral PZT. Figure 4a ($x=0$) only contains spots associated with the fundamental perovskite lattice diffraction and there is no evidence of superlattice reflections. However, Fig. 4b, c, and d show, superlattice reflections at the $\{h + 1/2, k + 1/2, l + 1/2\}$ positions. These reflections arise as a result of antiphase rotations of the O octahedra around the polar axis [17, 19]. In compositions where

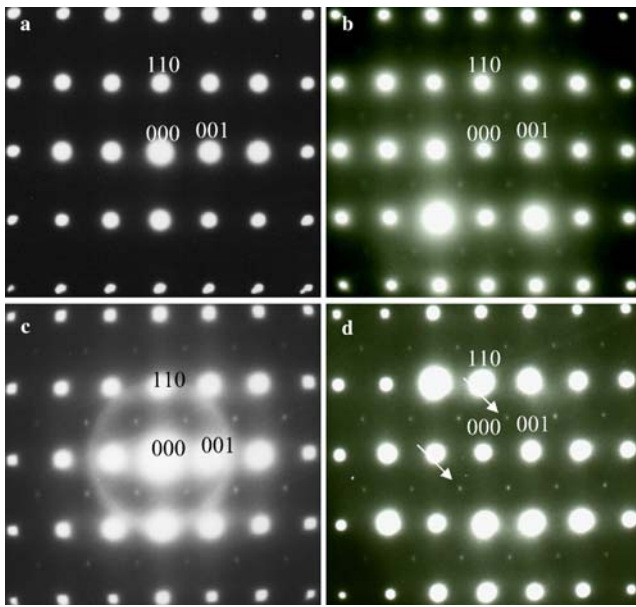


Fig. 4 a–d Electron diffraction patterns along the pseudocubic $\langle 110 \rangle$ zone axes of MPB samples as a function of Sr^{2+} concentration in $\text{Pb}_{(1-x)}\text{Sr}_x\text{ZrTiO}_3$ for $x=0, 0.08, 0.12, 0.16$. Superlattice reflections of the type $1/2\{000\}$ associated with antiphase tilting are *arrowed*, after Zheng et al. [17]

$x=0.08$ and 0.12 , the intensities associated with the superlattice reflections are diffuse and no long range correlation of tilt occurs. In contrast, the reflections observed in samples where $x=0.16$ are stronger and discrete, implying long range interaction [17]. It is proposed that for samples where $x=0.16$, the octahedral tilt transition causes a long-range structural distortion which results in an increase in the strain energy of domain walls and therefore activation energy for domain wall motion [17]. This would give rise to a smaller extrinsic contribution to d_{33} . The short range ordered tilting in samples where $x=0.08$ and 0.12 will not cause further macroscopic distortion of the structure, neither increasing the strain energy of the domain walls nor their activation energies for motion [17].

It is interesting to note that the superlattice reflections in Fig. 4b, c, and d are identical to those in Fig. 2b, both arising due to antiphase rotations of the O-octahedra. The substitution of Sr on the A-site has therefore increased the octahedral tilt transition for MPB compositions to above room temperature. This argument is substantiated by considering that the tolerance factor, t , decreases from 0.99 to 0.98 as the Sr concentration increases, where,

$$t = (R_A + R_O) / \sqrt{2}(R_B + R_O)$$

and R_A , R_B and R_O are the ionic radii of the average A-, B- and O-sites. As discussed extensively by Reaney et al. [20] in their study of Sr and Ba based complex perovskites,

the onset of octahedral rotations in antiphase is likely to occur above room temperature for perovskite-structured ceramics whose tolerance factor is <0.985 .

4 BiMeO₃-PbTiO₃ solid solutions

In the BiMeO₃-PbTiO₃ family of solid solution three distinct formulations show bulk properties suitable for commercial exploitation, 0.64 BiScO₃-0.36 PbTiO₃, (T_c 450°C, $d_{33} \sim 450$ pC/N) [5]) BiMg_{1/2}Ti_{1/2}O₃ - PbTiO₃ ($T_c=$ 420°C, $d_{33}=220$ pC/N, [7]) and Bi(Sc_{1/2}Fe_{1/2})O₃-PbTiO₃ ($T_c=$ 440°C, $d_{33}=300$ pC/N, [21]). Randall et al. and [6, 22] Woodward et al. [23, 24] studied the domain structure of several BiMeO₃-PbTiO₃ specifically to compare and contrast the observed changes in structure and domain structure to those across the MPB in the PZT system. Here, the data by Randall et al. [6] is reproduced for the BiScO₃-PbTiO₃ solid solution.

Figure 5 shows the domain structures/microstructure associated with different nominal compositions in the BiScO₃-PbTiO₃ dielectric phase field diagram [6]. Figure 5a, nominally obtained from a ceramic within the R phase field, shows small perovskite grains and some secondary phases, notably Sc₂O₃, consistent with the earlier X-ray diffraction studies [5]. As BiScO₃ content decreases, the perovskite phase becomes progressively thermodynamically more stable. In the MPB region between R and T phases, the perovskite phase has grains or crystallites ~ 0.5 μm and contains non-180° domain structures which twin on $\{110\}$ planes in a zig-zag configuration, Fig. 5b, frequently observed with rhombohedral ferroelectric perovskites [25]. In addition, weak systematic perturbations in contrast are observed within the grains, hereafter termed a ‘sub-domain structure.’ Figure 5c and d show domain structures in the tetragonal ferroelectric phase field. Here 90° domain wall structures are observed, together with 180° domain walls. The 90° domains, when inclined with respect to the electron beam, give rise to δ -fringes, and the 180° walls have α -fringe contrast [26]. Figure 5d shows in bright field the α -fringe of the 180° domain wall. The domain walls are pinned by the ferroelectric 90° domain walls. In summary, the domain structures in the BiScO₃-PbTiO₃ have domain morphologies and configurations very similar to PZT.

The properties of BiScO₃-PbTiO₃ solid solutions are optimised at the MPB with a high piezoactivity (450 pC/N) with respect to T_c (450°C). This suggests a strong extrinsic contribution to the piezoelectric and electromechanical coupling coefficients. The R phase immediately adjacent to the MPB has space group R3m and not even electron diffraction reveals evidence of octahedral rotations associated with the R3c phase. The positive effect of Sr substitution on the extrinsic piezoelectric properties of PZT is catastrophi-

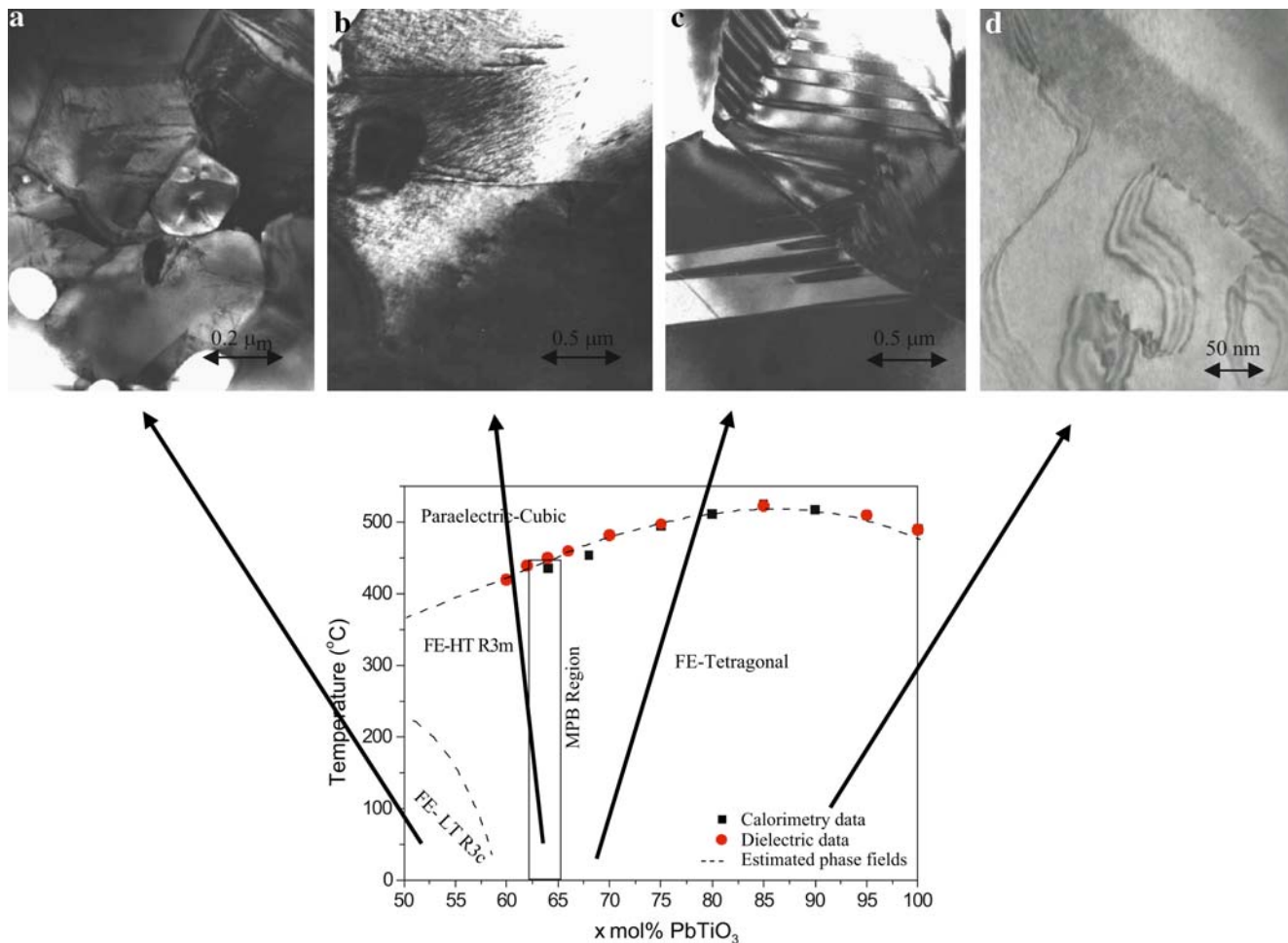


Fig. 5 a–d Domain structures/microstructure associated with different nominal compositions in the $\text{BiScO}_3\text{-PbTiO}_3$ dielectric phase field diagram, after Randall et al. [6]

cally reversed when long range octahedral rotations are induced above room temperature. The absence of the R3c phase at the MPB may therefore be significant for optimising piezoelectric properties in this system as well as in PZT based ceramics.

5 Aurivillius phases

Aurivillius phase are layered structures in which $n(\text{A,Bi})\text{MeO}_3$ (where $\text{A}=\text{Ca, Sr, Ba}$ and $\text{Me}=\text{W, Ti, Nb, Ta}$) perovskite blocks are separated and sheared along $1/2\langle 111 \rangle$ by Bi_2O_3 fluorite structured layers [27]. They are generally orthorhombic, with the exception of $\text{Bi}_4\text{Ti}_3\text{O}_{12}$ which is considered monoclinic, and odd and even values of n have space groups, B2cb and Ama2, respectively [28]. The value of n varies between 1 and 5 depending on stoichiometry and T_c varies in accordance with the tolerance factor of the perovskite block [29]. Consequently, the compound with the highest recorded T_c is $\text{CaBi}_2\text{Nb}_2\text{O}_9$, as predicted by Suarez

et al. [29] and reported by Yan et al. [30]. In stoichiometric Aurivillius phases, the amplitude of rotation of the octahedral cages is coupled to the polarisation along the a -axis. In addition, Reaney et al. [31] proposed that several stoichiometric compounds exhibit intermediate phases, between the low temperature ferroelectric and high temperature prototype, $I4/mmm$ phase. The intermediate phases were considered to be distorted to orthorhombic as a result of octahedral rotations but para—rather than ferroelectric. In later work, Hervoches et al. [32, 33] and Zhou et al. [34] confirmed using X-ray and neutron diffraction the presence of these intermediate compounds with Amam symmetry in several Aurivillius phases with the characteristics initially suggested by Reaney et al. [31] based on in-situ electron diffraction. Figure 7a and b show similar patterns from a grain of $\text{SrBi}_4\text{Ti}_4\text{O}_{15}$ (SBTO_{15}) to those initially reported by Reaney et al. [31]. The electron beam is parallel to the $[010]_o$ (where o =orthorhombic) zone axis and diffracted images are recorded at 23 and 650°C, respectively. Figure 6a shows a typical distribution of maxima common-

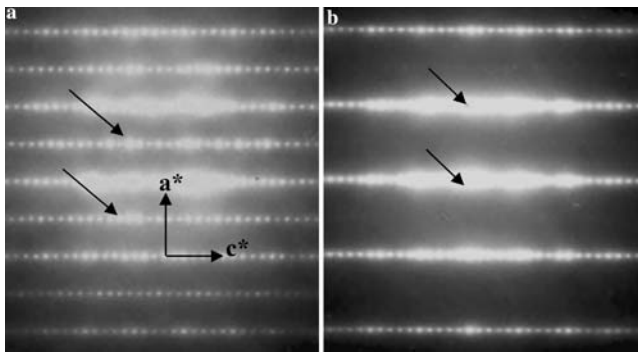


Fig. 6 **a** and **b**. Electron diffraction patterns from a grain of SBTO_{15} similar to those initially reported by Reaney et al. [31]. The electron beam is parallel to the $[010]_o$ zone axis and diffracted images are recorded at 23 and 650°C, respectively. The rows of superlattice reflections associated with octahedral tilting and fundamental spots are arrowed in **a** and **b**, respectively

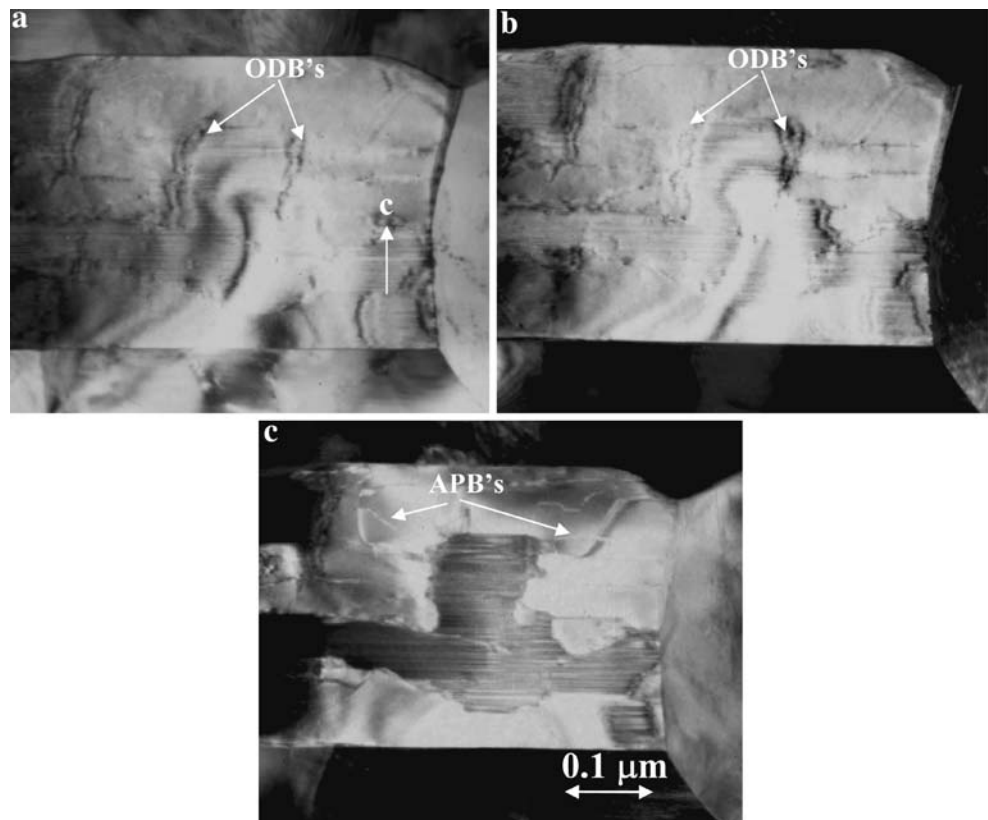
ly observed with bismuth titanate-based materials. The weaker systematic rows (arrowed in Fig. 6a) are associated with rotations of the octahedra that double the unit cell in the a,b plane [10]. As the temperature increases, the systematic rows become less intense until they are no longer visible at a temperature approximately 150°C above the ferroelectric phase transition (570°C) [31].

Figure 7a, b and c are TEM images recorded at room temperature and obtained with the electron beam parallel to the $[010]_o$ of a grain in an SBTO_{15} ceramic, first presented

by Reaney and Damjanovic [35]. Figure 7a is a bright field (BF) image of the grain whereas Fig. 7b and c are dark field (DF) images obtained using the fundamental, intense systematic row and the weaker superlattice row, respectively. There are many types of planar defects apparent in these images. Stacking errors in perovskite-layer structures are quite common and these are invariably observed to occur perpendicular to the c -axis [31] and are visible in all the images. More importantly however, is the observation of inclined planar defects marked as ODB's which exhibit asymmetric fringes in BF and symmetric in DF, Fig. 7a and b, respectively. This is termed δ -fringe contrast and its appearance is consistent with the presence of ODB's [26]. In Fig. 7c the illuminated regions give rise to the superlattice reflections and their edges are coincident with the appearance of the δ -fringes in Fig. 7a and b. In addition, within the bright contrast in Fig. 7c, a second type of planar defect can be observed. The imaging conditions and their morphology define them as APB's which separate translational domains [26].

The temperature of disappearance of the superlattice reflections in Fig. 6 is 150°C higher than the ferroelectric phase transition. No other ferroelectric phenomenon is observed in this material and therefore the phase transition, giving rise to the APB's and ODB's, is considered to be a transformation to an intermediate paraelectric state [35]. Furthermore, ODB's may only arise if there is a change in

Fig. 7 TEM images from a grain of SBTO_{15} at room temperature in an SBTO_{15} ceramic, obtained with the electron beam parallel to the $[010]_o$. **a** is a bright field image, **b** is a dark field image obtained using fundamental reflections and **c** is a dark field image obtained using the superlattice rows indicated in Fig. 6a, after Damjanovic and Reaney [34]. ODB=orientation domain boundary, APB=anti-phase domain boundary



crystal class and a doubling of the unit cell, i.e. if the intermediate structure is orthorhombic. This demonstrates that there is a phase transition from tetragonal to orthorhombic which occurs at a temperature above that of the ferroelectric phase transition [35]. The room temperature phase of SBTO_{15} is known to be orthorhombic and therefore the paraelectric (PE) to ferroelectric (FE) phase transition must occur within the same crystal class [35]. The phase transition sequence can thus be written as:

tetragonal (PE) – orthorhombic (PE) – orthorhombic (FE)

with only 180 inversion domains allowed to form at the PE-FE phase transition. It is likely however that at the PE-FE transition the polarisation vector will align along the directions dictated by the strain tensor associated with pre-existing domains from the non-ferroelectric phase transition. In effect, the higher temperature ferroelastic domains become the ferroelectric non-180° domains [35]. Hervoches et al. [32, 33] and Zhou et al. [34] have confirmed this phase transition sequence in several common Aurivillius phases.

In order for these domains to be piezoelectrically active, the movement of the domain wall must be accompanied with a change in polarization [35]. This may be energetically difficult in SBTO_{15} since their movement requires the rearrangement of octahedral rotations. The effect of the octahedral rotations on the piezoactivity of PZT based ceramics is demonstrated in Section 2. Here, Fig. 8 shows the piezoelectric coefficients for SBTO_{15} and Nb doped $\text{Bi}_4\text{Ti}_3\text{O}_{12}$ (BTO_{12} -NB) as a function of the amplitude of the AC pressure. The large increase of d_{33} with pressure in BTO_{12} -Nb indicates strong irreversible contributions from non-180° domain walls [1]. In contrast, SBTO_{15} shows no significant change in piezoactivity as a function of increasing pressure, suggesting that irreversible domain wall motion is inhibited. Although polarisation and octahedral rotations are also coupled in BTO_{12} , this compound has a second polarisation vector along the *c* as well as *a*-axis which may allow irreversible motion of the domain wall and therefore threshold behaviour in the piezoelectric response as a function of applied stress.

6 General discussion and conclusions

Until recently, perovskite and related piezoelectric compounds had only been considered from the perspective of materials that undergo a FE to PE phase transitions. No consideration was given to the fact that in many compounds two or more phase transitions may occur on cooling. The most common type of phase transition in perovskites and related compounds arise as a result of rotations of the O octahedra around principle axes [36]. Glazer [19], in his

early work, stated that compounds which undergo ferroelectric as well octahedral tilt phase transitions on cooling exhibit coupling between the polarisation vector and crystallographic direction around which O-octahedra rotate. Given that piezoelectricity in its simplest description is a coupling of polarisation and strain, it is inevitable that octahedral tilt transitions will influence piezoelectric and electromechanical coupling coefficients in the manner described in Sections 2, 3, 4. The strength of coupling between tilt and ferroelectric phase transitions depends on many factors such as the amplitude of rotation and correlation length of the tilted regions. The onset temperature of a tilt transition and the amplitude of rotation at room temperature are controlled by the tolerance factor [20]. This is true across a broad range of compounds, from Sr and Ba based complex perovskites to PZT in which tilt only occurs in the low *t*, Zr rich part of the phase diagram [12, 20]. In general, Pb and Ba based ferroelectrics do not undergo tilt transitions above room temperature, notable exceptions are PZT, $\text{Zr} > 0.8$ and possibly $\text{PbY}_{1/2}\text{Nb}_{1/2}\text{O}_3$. As a consequence, tilt transitions impact infrequently on most ferroelectric studies. However, Bi based compounds (simple perovskites and Aurivillius compounds) are receiving increasing attention for their ferroelectric/magnetic properties, as ferroelectric thin films, as potential PbO free replacements for conventional piezoelectrics and as high T_c piezoelectrics. Bi^{3+} is a highly polarisable, small, lone electron pair ion which in most BO_6 octahedral frameworks will induce octahedral tilting as well as ferroelectric phase transitions above room temperature. Section 4 demonstrated that tilt the transition cannot be ignored if the properties of Aurivillius phase are to be understood. The new generation of BiMeO_3 simple perovskite will need to be viewed in the same light, e.g. BiFeO_3 has space $R3c$ in which the octa-

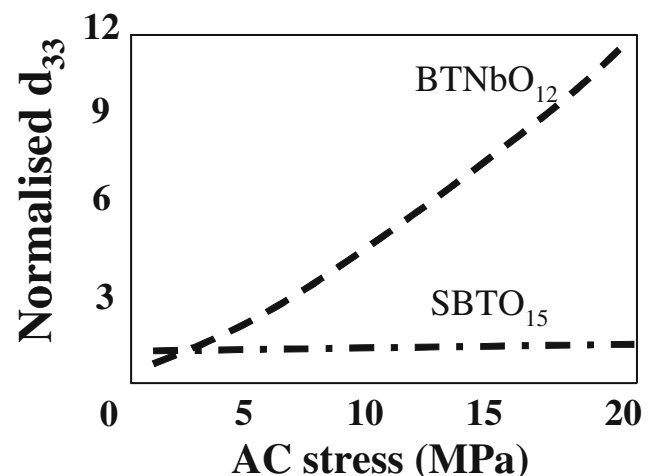


Fig. 8 Normalised piezoelectric coefficient (d_{33}) for SBTO_{15} and Nb doped BTO_{12} as a function of the amplitude of AC pressure, after Damjanovic and Reaney [34]

hedra are rotated in antiphase around the [111] direction. Moreover, the metastable compounds, BiMnO_3 , BiAlO_3 , BiScO_3 , $\text{BiMg}_{1/2}\text{Ti}_{1/2}\text{O}_3$, may exhibit tilt transitions which will even persist for a substantial compositional range in solid solution with PbTiO_3 , as recently discussed by Eitel et al. [5]. The low tolerance factors of these compounds may even induce antiferroelectric rather than ferroelectric coupling, as observed in PbZrO_3 .

References

1. Q.M. Zhang, W.Y. Pan, S.J. Jang, L.E. Cross, *J. Appl. Phys.* **64**, 6445 (1988)
2. Q.M. Zhang, H. Wang, N. Kim, L.E. Cross, *J. Appl. Phys.* **75**, 454 (1994)
3. G. Arlt, N.A. Pertsev, *J. Appl. Phys.* **70**, 2283 (1991)
4. T. Takenaka, K. Sakata, *J. Appl. Phys.* **55**, 1092 (1984)
5. R.E. Eitel, C.A. Randall, T.R. Shrout, et al., *Jpn. J. Appl. Phys. Part 1, Regular Papers Short Notes & Review Papers* **40**(10), 5999 (2001)
6. C.A. Randall, R.E. Eitel, T.R. Shrout, et al., *J. Appl. Phys.* **93**(11), 9271 (2003)
7. R.E. Eitel, C.A. Randall, T.R. Shrout, et al., *Jpn. J. Appl. Phys. Part 1, Regular Papers Short Notes & Review Papers* **41**(4A), 2099 (2002)
8. H. Shulman, D. Damjanovic, N. Setter, *J. Am. Ceram. Soc.* **83**(3), 528 (2000)
9. E.K.H. Salje, *Phase Transitions in Ferroelastic and Co-Elastic Crystals*. (Cambridge University Press 1990)
10. B. Noheda, D.E. Cox, G. Shirane, J.A. Gonzalo, L.E. Cross, S.-E. Park, *Appl. Phys. Lett.* **74**(14), 2059–2061 (1999)
11. A.M. Glazer, *J. Conf. Abstr.* **8**, 137 (2003)
12. D.I. Woodward, J. Knudsen, I.M. Reaney, *Phys. Rev., B* **72**, 104–110 (2005)
13. R. Schierholz, R. Thiesman, H. Kungl, H. Fuess, *Acta Crystallogr.* **A61**, C400 (2005)
14. D. Damjanovic, *J. Am. Ceram. Soc.* **88**, 2663 (2005)
15. S.K. Ragini Mishra, D. Pandey, H. Lemmens, G. Van Tendeloo, *Phys. Rev., B* **64** (2001)
16. R. Ranjan, S.K. Ragini Mishra, D. Pandey, B.J. Kennedy, *Phys. Rev., B* **65** (2001)
17. H. Zheng, I.M. Reaney, W.E. Lee, N. Jones, H. Thomas, *J. Am. Ceram. Soc.* **85**(9), 2337–2344 (2002)
18. H. Zheng, I.M. Reaney, W.E. Lee, N. Jones, H. Thomas, *J. Uro Ceram. Soc.* **21**, 1371–1375 (2001)
19. A.M. Glazer, *Acta Crystallogr.* **B28**, 3384–3392 (1972)
20. I.M. Reaney, E.L. Colla, N. Setter, *Jpn. J. Appl. Phys.* **33**, 3984–3990 (1994)
21. I. Sterianou, I.M. Reaney, D.C. Sinclair, D.I. Woodward, D.A. Hall, A.J. Bell, T.P. Comyn, *Appl. Phys. Lett.* **87**(24):Art. no. 242901 (2005)
22. C.A. Randall, R. Eitel, B. Jones, T.R. Shrout, D.I. Woodward, I. M. Reaney, *J. Appl. Phys.* **95**(7), 3633–3639 (2004)
23. D.I. Woodward, I.M. Reaney, R.E. Eitel, C.A. Randall, *J. Appl. Phys.* **94**(5), 3313–3318 (2003)
24. D.I. Woodward, I.M. Reaney, *J. Phys.-CM* **16**(49), 8823–8834 (2004)
25. C.A. Randall, D.J. Barber, R.W. Whatmore, *J. Mater. Sci.* **22**(3), 925–931 (1987)
26. W.E. Lee, I.M. Reaney, M.A. McCoy, *Brit. Ceram. Proc.* **55**, 199–212 (1995)
27. B. Aurivillius, *Ark. Kemi* **59**, 499 (1949)
28. R. Newnham, R. Wolfe, J. Dorrian, *Mater. Res. Bull.* **6**, 1029 (1971)
29. D.Y. Suarez, I.M. Reaney, W.E. Lee, *J. Mater. Res.* **16**(11), 3139–3149 (2001)
30. H.X. Yan, H.T. Zhang, M.J. Reece, X.L. Dong, *Appl. Phys. Lett.* **87**(8): Art. no. 082911 (2005)
31. I.M. Reaney, M. Roulin, H.S. Shulman, N. Setter, *Ferroelectrics* **165**, 295–305 (1995)
32. C.H. Hervoches, J.T.S. Irvine, P. Lightfoot, *Phys. Rev., B* **64**(10): Art. no. 100102 (2001)
33. C.H. Hervoches, A. Snedden A., R. Riggs, S.H. Kilcoyne, P. Manuel, P.J. Lightfoot, *Solid State Chem.* **164**, 280–291 (2002)
34. Q.D. Zhou, B.J. Kennedy, C.J. Howard, *Chem. Mater.* **15**(26), 5025–5028 (2003)
35. I.M. Reaney, D. Damjanovic, *J. Appl. Phys.* **80**(7), 4223–4225 (1996)
36. H.D. Megaw, *Crystal Structures: A Working Approach*. (W. B. Saunders, Philadelphia/London/Toronto)